SAKARYA ÜNİVERSİTESİ
FEN BİLİMLERİ ENSTİTÜSÜ DERGİSİ

Sakarya University Journal of Science
SAUJS

e-ISSN 2147-835X Period Bimonthly Founded 1997 Publisher Sakarya University
http://www.saujs.sakarya.edu.tr/

Title: Aeroacoustic Simulation of an Owl Wing Cross-Section Using Computational Fluid Dynamics

Authors: Ferit YILDIZ, Sedat TOKGOZ

Recieved: 2021-07-09 00:00:00

Accepted: 2022-03-16 00:00:00

Article Type: Research Article

Volume: 26
Issue: 2
Month: April
Year: 2022
Pages: 375-387

How to cite
Ferit YILDIZ, Sedat TOKGOZ; (2022), Aeroacoustic Simulation of an Owl Wing Cross-Section Using Computational Fluid Dynamics. Sakarya University Journal of Science, 26(2), 375-387, DOI: 10.16984/saufenbilder.968701
Access link
https://dergipark.org.tr/tr/journal/1115/issue/69580/968701

Sakarya University Journal of Science 26(2), 375-387, 2022

Aeroacoustic Simulation of an Owl Wing Cross-Section Using Computational Fluid Dynamics

Ferit YILDIZ*[1], Sedat TOKGOZ[1]

Abstract

In this study, we aim to investigate the low noise flights of owls in terms of aerodynamics. The flow around cross-section of an owl wing, which is known for its nearly silent flight, is numerically analyzed using Computational Fluid Dynamics (CFD). The analysis are based on the parameters of angle of attack and the flight speed. The aerodynamic effects on the acoustic is compared in terms of vorticity and sound pressure level, where the frequency interval for the acoustic data is set to 0-7500Hz. It was seen that the vortical organisations around the airfoils are closely related to the acoustic results. The results show that the increase in both velocity and angle of attack affect the vorticity, thus lead to a rise in sound pressure level. It can be stated that the owl airfoil shape ensures a relatively silent flight.

Keywords: Aerodynamics, airfoil, biological flow, Computational Fluid Dynamics

1. INTRODUCTION

The noise of aircrafts is a significant problem for the environment. Different solutions for developing low-noise aircrafts are investigated in the industry. Consequently, one of the best application of these subjects probably lies in nature itself. Birds, which are responsible for the desire of flying, are analyzed for further improvements in aviation [1, 2]. As a result of this, various properties of birds were implemented into aircraft designs to achieve new improvements in terms of aerodynamic, as well assilent flight [3].

The wings of birds are adapted to operate over a wide range of flight styles, from the highly rigid geometries for gliding to the relatively flexible kinematics for flapping [4, 5]. These flight styles are extended further during take-off, landing, and manoeuvering while flying at high angles of attack and generating highly unsteady flows. In most of the cases, all of these occur in turbulent flow conditions. Not only the flight style, also the physical appearance/feature of the wings play a critical role in the flight itself. For example, they can vary from narrow to wide wings or from sharp to rounded forms [4, 6, 7] Compared to narrow wings, wide wings can help a bird to glide longer at low flight speeds. Furthermore, to carry the prey up in the air, larger and wider wings provide additional lift [8]. If we focus on owls, relatively large, broad, rounded wings, with a large surface area relative to their weight, are seen. This low wing-load (body mass × 9.81 ms-2 / both wing areas) allows them to fly easily, without much

* Corresponding author: ferit.yldz@hotmail.com
[1] Gebze Technical University
E-mail: sedattokgoz@gtu.edu.tr
ORCID: https://orcid.org/0000-0002-7450-846X, https://orcid.org/0000-0002-0836-2861

flapping. They can glide for long periods, even at low flight speeds [9, 10].

Owls are known for their silent flights. They are using their hearing system to sense prey, therefore they need to reduce flight noise. Flying slowly is one choice, but to provide enough lift at low-speed, the wing needs to be highly cambered [11]. In comparison to other similar birds, the owl wing cross-section profile shows a special camber and thickness distribution, which provides enough lift at low flight speed [12]. Considering this, together with the large wing area of owl wings, the special features (high camber, thinner profile towards trailing edge) are distributed throughout the whole wing, which makes the owl a nearly silent flying bird.

Neuhaus et al. [13] examined the flight noise of a tawny owl (Strix aluco) and a mallard duck, with and without the serrations on the leading edge. The recorded noise during flight reaches its most intense range between 200 and 1500 Hz. Furthermore, wind tunnel experiments show that the flow over the owl wing has a more laminar flow character compared to the flow over wing of the duck and has lower flight noise with the serrations on the leading edge Ito [14] investigated a NACA63-414 profile with different number of teeths as serrations and two Reynolds numbers ($2.1x10^4$ and $2.1x10^5$) to show the behavior of the flow at low and high speeds. By increasing the number of teeth on the wing, it is seen that the aerodynamic performance is improved in the low Reynolds number region, in turn, no significant changes are seen for the high Reynolds number region. Also, Mascha [15] mentioned the serrations on owl wings and identified the outstretched pennula (hair-like extensions of the feather) as a source of the mild wing layer of owls, which reduces the flight noise. Hertel [5] derived an explanation of how the velvet-like upper surface may prevent generated sound. He claimed that it acts as a kind of cushion so that it reduces the noise during flight.

Geyer et al. [16] performed wind tunnel and outdoor measurements to demonstrate the difference between the noise levels of the owl compared to the noise of non-silently flying birds. The outdoor experiment was carried out with an owl, flying over a microphone array. The wind tunnel measurements were performed with prepared wings (real wings of dead birds) of an owl, hawk, and kestrel at fifteen flight speeds between 5 m/s and 20 m/s at 0°, 8°, and 16° AOA. The outdoor flight noise was recorded between 500 Hz and 10 kHz frequencies. The results of both experiments show that the owls generate less noise (60dB) than the other birds (75-90dB) used in the studies. No major noise difference was measured at low-frequency level. But for mid and high-frequency range, the owl outperformed the other birds in case of silence.

In addition to the whole body or wing studies, investigations on 2D wing profiles can be found in the literature. Kondo et al. [17, 18] investigated the effect of the flow detachment around an airfoil (owl-like profile on the lift and drag coefficients using CFD. They concluded that the owl airfoil has a higher lift/drag ratio compared to NACA0002, NACA0012, and the Ishii airfoil. Anyoji et al. [19] performed experiments in the wind tunnel with an owl-like airfoil, where they visualized the flow and measured the lift and drag properties. Again, the high cambered airfoil (on the pressure side) showed a better lift/drag ratio compared to NACA0012.

It is shown in the literature that carrying out acoustic experiments with living animals are mostly difficult, whereas body part samples are also hard to find [6, 12, 16]. Since the owl is well known for its nearly silent flight, the scope of this work is to numerically investigate the owl wing cross-section in terms of aerodynamics and aeroacoustics to obtain faster, and reasonable acoustic results, compared to experiments. Properties like flight speed and Angle of Attack (AoA) were investigated to understand the flow behavior in relation to the reported silent flight characteristics. The connection between vortices and acoustics were examined to realize the noise generation of the owl flight.

2. NUMERICAL SET-UP AND DESIGN

In this section, the setup of the numerical analysis will be described, whereas a brief explanation about the design and meshing process will be

explained. All numerical analysis in this paper were performed using ANSYS Fluent software.

2.1. Computational Details

2.1.1. Turbulence Model

For simple cases of turbulent flow, equations can be solved directly, whereas, in complex turbulent flows, CFD simulations predict the outcome of turbulence with the help of turbulence models. These turbulence models are simplified equations that predict the statistical formation of turbulent flows [20]. In order to choose the most suitable turbulence model, the case which is going to be solved must be defined properly. Two common approaches can be seen in CFD, which are Large-eddy simulation (LES) and Reynolds-averaged Navier-Stokes (RANS). LES is a transient technique in which the large eddies are resolved directly, while small eddies are modeled. On the other hand, the RANS use the Navier-Stokes equations (as time-averaged) without filtration, while Reynolds stresses are solved directly [21]. Remaining turbulence models are based on these two approaches [22].

RANS and LES models have their pros and cons. In comparison to RANS models, LES is able to predict the vortex shedding and flow recirculation accurately. In contrast, LES has to be run for a sufficiently long flow-time to obtain a stable solution and can only be applied to 3D models. This leads to computational costs, which are higher than that of the steady RANS calculations. On the other hand, Detached-Eddy-Simulation (DES), which is a hybrid LES-RANS model. This model uses the RANS for the wall limited flows, whereas the LES for the far-field. The DES model requires more computational costs than RANS but requires less than LES [21, 22].

Spalart-Allmaras is a low Reynolds number turbulence model, which is developed for aerodynamic applications. This model has some weakness in computing shear flow, separated flow, or decaying turbulence, but it's advantageous in terms of convergence and stability [22]. For example X. Liu and X. Liu [23] used this model in the steady flow over an owl-wing-based airfoil for pressure and velocity coupling. The Spalart-Allmaras model has been shown to realize decent results for applications involving wall-restricted flows and boundary layers subjected to reverse pressure gradients [24]. Therefore, the Spalart-Allmaras was selected for the steady analysis as turbulence model. The DES, with Spalart-Allmaras as a submodel, was chosen for the transient cases, because of its capabilities of solving the wall-bounded and far-field flows better than RANS models. The submodel decision was made so that the analysis all have the same RANS model. In general, better vortex shedding and turbulence resolution was obtained compared to RANS, whereas computational costs were much less than LES.

2.1.2. Acoustic Model

There are different approaches to calculate the aeroacoustic field from flow field,where in Lighthill's acoustic analogy, Lighthill generated a wave equation by using the Navier-Stokes and continuity equations. This approach not only consists of the generated noise, but also includes the flow convection and the gradual dissipations by conduction and viscosity [25]. Unfortunately, Lighthill's analogy cannot describe kinematic effects, because refraction at shear- or boundary layers appear as sources. Several generalized wave equations have been derived after Lighthill, in the attempt to isolate those drawbacks, which could be stated as true sources of the sound [25, 26].

An essential part of aeroacoustics is the sound source characteristics. Consequently, it is important to understand the monopole, dipole, and quadrupole sources, which are very important to explain aerodynamically generated noise. The monopole is defined as a single, spherical sound source which radiates waves inward or outward. On the other hand, the dipole can be realized as two out of phase monopoles with the same strength, where the quadrupole is alike and consists of two out of phase dipoles [27]. This forms the basis to describe the relation between noise and flow. Both vortex and monopole have a direction, a strength and are based on velocity,

whereas they also can interact with each other and form new structures. While monopoles form new type of sources (dipole, quadrupole), the same situation occurs also in vortices, which can form complex structures by affecting one another.

ANSYS Fluent offers one acoustic source equation, the Ffowcs-Williams & Hawkings (FW-H) wave equation. In general, it takes the Lighthill's equation as a base, where a control surface is used to retain the monopole and dipole sources. Despite that, the effect of quadrupole sources, which are outside of the control surface, can be added with the Lighthill Tensor [26]. Combining this acoustic model with the DES turbulence model, the aeroacoustic behavior of the owl wing profile is described in terms of sound pressure (dB).

2.2. Design, Mesh, Numerical Setup, and Flow Conditions

2.2.1. Design

It is hard to define a standard 2D profile for avian wings, since they vary from bird to bird, from species to species. Different methods are used to define standard profiles for specific birds. In some studies, it is possible to find pairing approaches in which each bird's wing is associated with the most alike standard airfoil profile [28]. Others tried to scan a real wing and reproduce it in a computational environment. A 3D non-contact laser scanner[12], Projected pattern correlation technique [29], or a clinical tomography scanner are some of these kinds of methods [6].

For this study, the owl wing profile given by Liu et al. [12] is used as an airfoil profile (Figure 1) for the following CFD analysis. The owl profile is extracted from the cross-section at 40% of the wingspan.

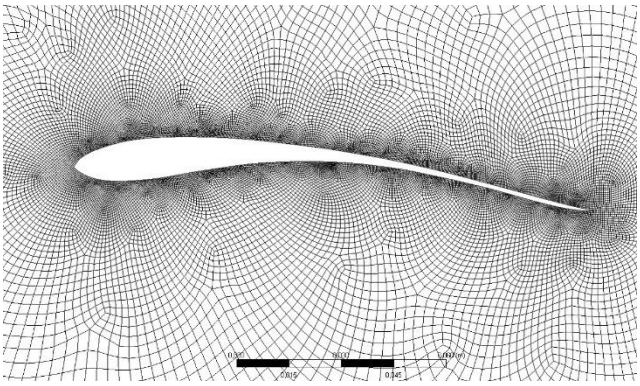

Figure 1 2D profile of an owl and the near-field mesh

2.2.2. Mesh

The mesh and the domain around the airfoil are shown in Figure 1 and Figure 2, respectively. The distances from the airfoils leading-edge to the upstream and downstream boundaries are 20x and 40x chords, respectively.

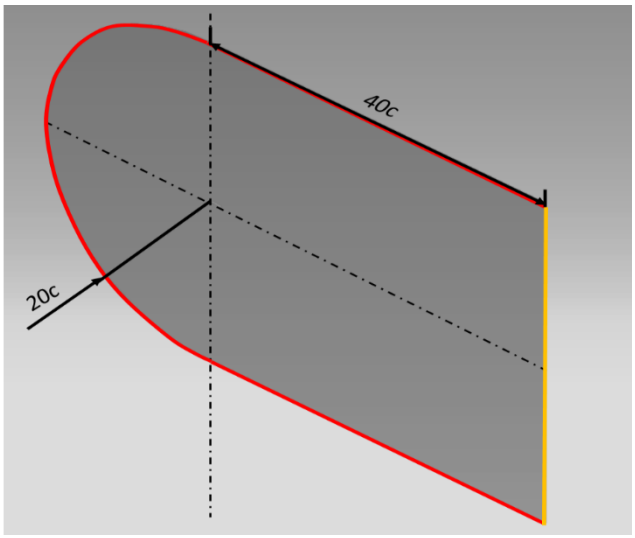

Figure 2 Domain of airfoil. Red line: inlet velocity boundary. Yellow line: pressure outlet boundary

The grid independency study shows five cases for possible meshing process (Table 1). The reference case is selected as case 4, where both near-field and far-field meshes are set as fine, relative to the first three cases. Since, the mesh around the airfoil had a poor resolution for case 1 and 2, the vortex shedding was affected in a negative way, which was the reason that these meshes were not suitable. On the other hand, case 3 had a finer

near-field mesh resolution, which was necessary for our study. It is found that the lower quality mesh in the far-field didn't affect the analysis in the near-field, since the main objective of this study was around the near-field. Due to limited computational resources, case 3 is determined as the optimal case instead of case 4 or case 5, where the mesh quality in the far-field is set between coarse and medium, whereas the near-field mesh quality is between medium and fine (case 3 in Table 1). The minimum grid size on the airfoil edge is 10^{-3}, while the average skewness is 0.13 and the average orthogonal quality is 0.97.

Table 1 Grid independency study

Case #	Nodes	Elements
1	9210	8934
2	18854	18557
3	26467	26501
4	31624	31231
5	39451	39070

2.2.3. Numerical Setup and Flow Conditions

According to Neuhaus et al. [13], the flight speed range of the owl is only about 6 to 10 m/s, where Mebs and Scherziger [9] stated that flight speeds of owls are in the range of 2.5 m/s to 7 m/s. Considering this, the maximum and minimum velocities investigated in this study are chosen as 2.5 m/s and 10 m/s. Additionally, 5 m/s is also selected to represent the medium speeds. Chord based Reynolds numbers are 2.6×10^4, 5.2×10^4, and 10.5×10^4. There is also a wide range of options for AOA, but 0°, 5°, and 10° were chosen according to gliding flight angles of owls [17, 18, 23, 30].

The same timestep number was selected for all cases to keep the same analyze period, which is important for studying the vortex shedding. For the vorticity results, the timestep is set to (Δt) 10^{-3}s, whereas an analysis for 2s is ensured. The numerical setup for the acoustic analysis depends on the Nyquist–Shannon sampling theorem. As stated by Sarradj et al. [31], at frequencies higher than 6.3 kHz the owl-generated noise couldn't be measured with microphones. Therefore, a max frequency of 7.5 kHz is considered sufficient for the acoustic analysis, which corresponds to a sampling frequency of 15 kHz. Here, a timestep value of $\Delta t = 6.6\times10^{-5}$s required, while the timestep number of 1.5×10^4 provides a flow time of 1s.

Vortex shedding is a significant mechanism which connects the aerodynamics and acoustics. The formation location, intensity and dimension (diameter) of different vortices lead to various sound pressure levels and noise locations in different frequency zones. Hereby, the vortices at specific instances should be analysed for this, which is the major reason of the unsteady incompressible flow analysis in this study [20, 22, 26].

Moreover, acoustic receivers are needed to be defined for the FW-H acoustic model. It is found in the literature that in wind tunnel measurements the receiver positions are located between 0.6-1 m from the airfoil, and distributed around the wing specimens at every 24 degrees [16, 32-34]. However, in numerical analysis, microphone distances and spacings are chord length based(e.g. 15x chord or 18x chord away from leading edge with 30° spacing) [23, 35]. In this study, the receiver placement is accomplished within a radius of 1.5 m from the leading-edge, which corresponds to 10 times the chord length, with an angular difference of 20˚ between the receivers. A total number of 18 receivers are placed around the airfoil as shown in Figure 3.

3. RESULTS

The results in this section are given in terms of vorticity and acoustic analysis for different freestream velocities and AoA's. The transient vorticity results are investigated in four equally spaced instant (0.5 seconds between steps). The results of the intermediate steps are not shown for simplicity. The acoustic analysis of the owl flightwas performed in terms of sound pressure level (dB).

3.1. Vorticity

In order to understand the effects of the freestream velocities and AoA's to the flow behaviour, a general look at the topology of the flow is required. The results in Figure 3a-d show that the flow is relatively smooth and the vortices are periodical. Positive vortices form at an early point (compared to Figure 3e-h and Figure 3i-l) at the leading-edge pressure side, whereas the suction side flow is smooth and mostly attached to the boundary layer. Moving to the 5 m/s case (Figure 3e-h), both the positive and negative vortices became larger relative to the 2.5 m/s case (Figure 3a-d). Here, the vortices on the suction side get bigger in diameter. Also at the trailing-edge, an interaction between the negative and positive vortices can be seen more clearly. Comparing the two cases (Figure 3a-d and Figure e-h) at each time step, the flow pattern looks quite similar, especially the positive vortex pattern. The 10 m/s (Figure 3i-l) results contain larger vortices compared to those two cases, which is expected for increased velocities. Positive-negative vortex interaction can be seen on both sides of the airfoil, while at the suction side near the trailing-edge positive vortices force the flow to separate from an earlier point of the airfoil surface compared to other two cases. Furthermore, interactions of vortices intensify in the downstream of the trailing-edge. Because of the special camber structure of the owl profile , it is expected that the positive (clockwise) vortex shedding starts at a point near the leading edge of the profile, especially at small AOA's e.g 0°.

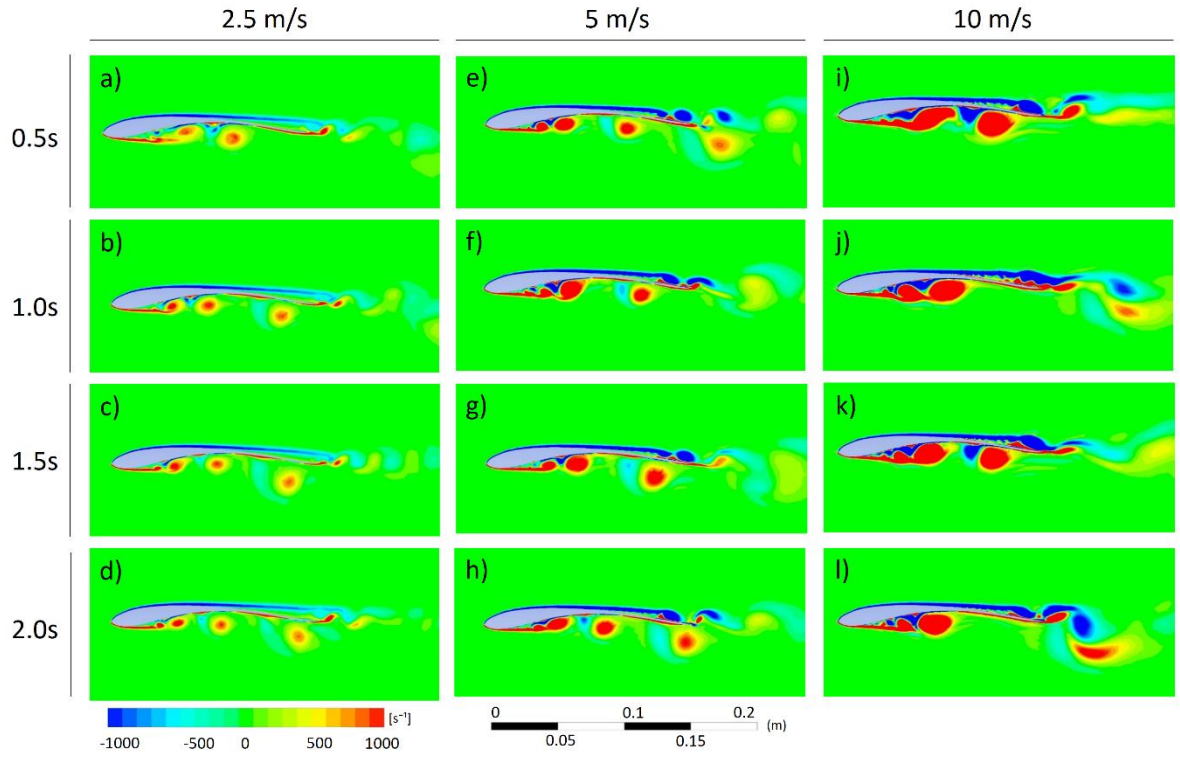

Figure 3 Vorticity distributions of AOA=0° for owl airfoil in four equally spaced instants

If we focus on the results of AoA=5° (Figure 4), the first point that stands out is the separation of the vortices at approximately the half chord length, whereas for the 0° AoA results (Figure 3) the separation point is closer to the trailing-edge (at approx. 75% of the chord). It can be concluded that this an outcome of the increase in AoA since the freestream velocity values didn't change. Another result of this change is that the negative vortices start to grow and get even larger than the positive vortices on the pressure side. For the 10 m/s case, at the suction side at 50% of the chord, the negative vortex grows over the positive vortex and traps it between the airfoil's surface. This indicates a separation bubble formation in the flow.

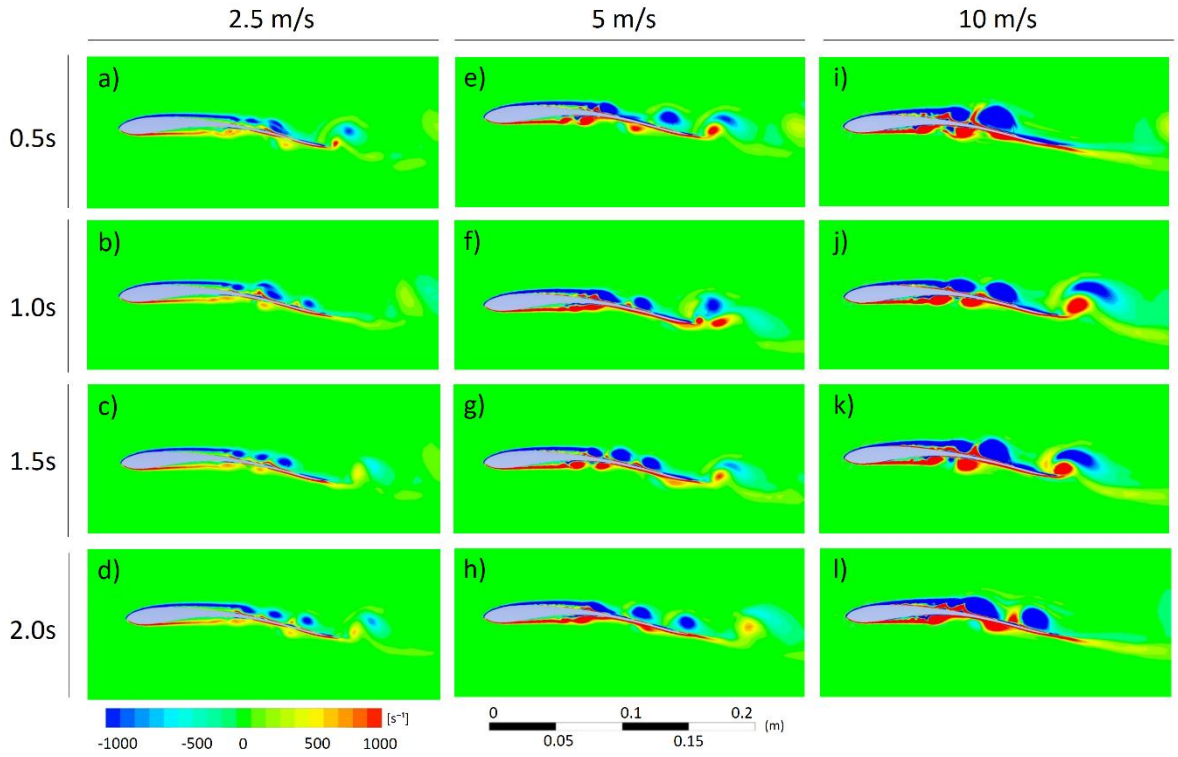

Figure 4 Vorticity distributions of AOA=5° for owl airfoil in four equally spaced instants

If we focus at the trailing-edge of the 5° case (Figure 4), the positive vortices on the pressure side initially move in a vertical direction, and then move in the downstream direction after interacting with the negative vortices. It can be due to the geometry of the owl airfoil's trailing-edge, which is sloping upward. Furthermore, different trailing edge geometries are seen in all three profiles. This leads to different interactions of vortices, which can affect the flow and the acoustic characteristics of each wing profile.

The results of AoA=10° cases are given in Figure 5. At this AoA the flow separate from an earlier point on the airfoil. The separation points of the negative vortices shift upstream to the leading-edge and reaches almost 25% of the chord length.. A similar effect is also seen in the 5° AoA cases (Figure 4).

In general, the 2.5 m/s cases (Figure 3) have small vortex shedding, while the 5 m/s and 10 m/s cases show rather greater vortex shedding. It is clearly seen that the airfoil is better adapted to the flow at 2.5 m/s. Because the flow stays attached at the pressure side at this velocity, which is the desired to produce lift more efficiently. Furthermore, it is also known that, in general the owls fly slower than other birds [9, 13].

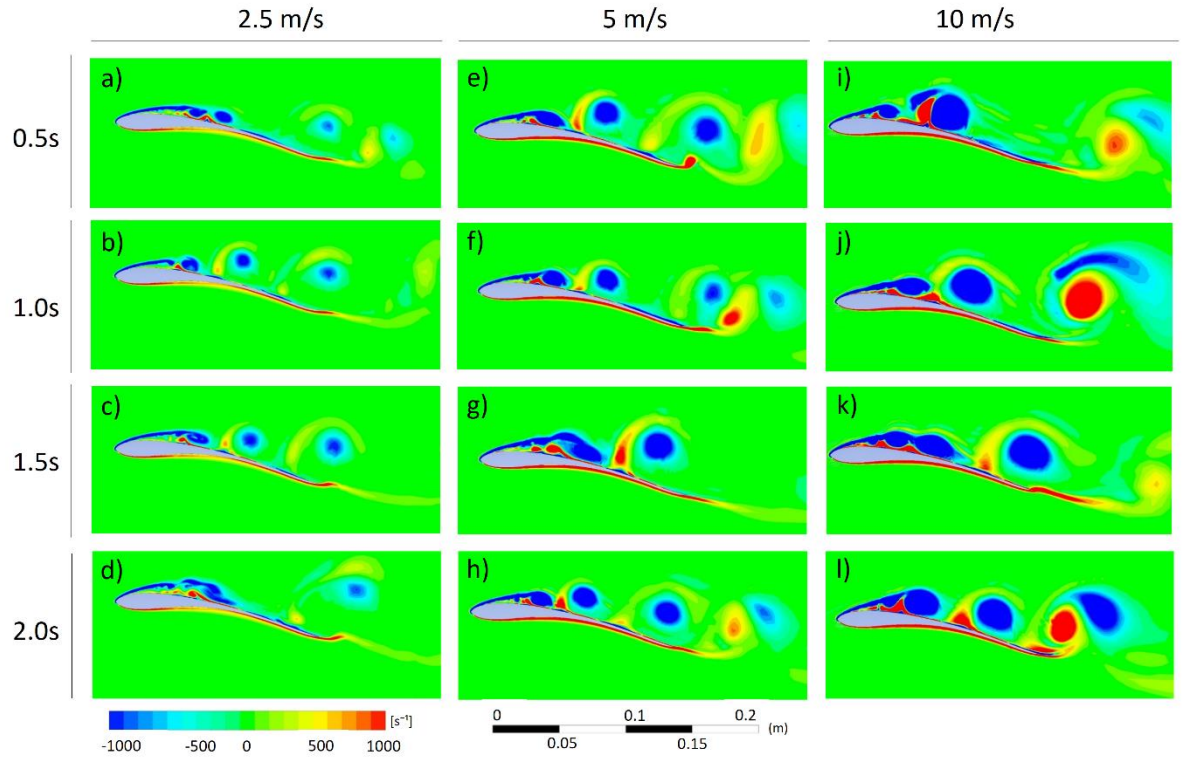

Figure 5 Vorticity distributions of AOA=10° for owl airfoil in four equally spaced instants

If we focus on the vortex dimensions, the diameter doubled from 2.5 m/s to 5 m/s, and almost tripled from 2.5 m/s to 10 m/s. Different from the other two cases, the 10° AOA results (Figure 5) demonstrate vortex interactions, which indicate the previously mentioned dipole and quadrupole sources. The image at 0.5s for the 10 m/s case (Figure 5i) is an example for dipoles, whereas image at 2.0s for the 10 m/s (Figure 5l) indicates a quadrupole. These sources are also seen in Figure 5e-h, while vortices with much smaller diameters are present in Figure 4e-h and Figure 4i-l.

3.2. Acoustic Results

In this section, the results of the acoustic analysis of the owl are investigated in terms of sound pressure level (dB). As mentioned in the previous chapter, the 5° (Figure 4e-l) and 10° (Figure 5e-l) cases are selected for aeroacoustic investigations. The aerodynamically generated noise is measured at the receivers, which are placed around the airfoil at a distance of 10 times the chord lengths (i.e. 1.5 m). The receivers are placed starting from the trailing-edge (0° receiver) and continues in a counter-clockwise direction with 20° increments (see Figure 7). First, similar to the literature [23, 31, 35] the acoustic data at the 0° receiver (Figure 6) is investigated to find the maximum sound pressure level in a range between 0-7500 Hz. After that, the maximum sound pressure level (SPL) is examined together with the remaining 17 receivers in a radar chart (Figure 7).

Following the approaches in the literature, the acoustic results in this section, are given relative to so-called “the reference acoustic pressure”. In the literature, it is defined as the threshold of hearing for humans and has a value of $2x10^{-5}$ Pa (=0 dB) [16, 36]. The negative sound pressure levels should be understood as values, which are below the reference acoustic pressure.

3.2.1. Sound Pressure Level

In Figure 6, the maximum SPL is located in a frequency interval of 20 - 120 Hz with a maximum SPL of 17dB for the case in Figure 4e-h. By increasing the velocity to 10 m/s, the SPL rises almost to 40dB for the same AoA. Here, the width of the SPL peak increases and propagates to a wider frequency range of 90 – 290 Hz. When

the AoA is increased to 10°, the effect of AoA on SPL can be clearly seen. The maximum SPL is around 25dB with a width of approximately 15-60 Hz for Figure 5e-h, and around 40dB at 40 – 170 Hz forFigure 5i-l.

At AoA=10°, the SPL decreases below the reference acoustic pressure level (RAPL) (i.e. 0 dB) around 2250 Hz. On the other hand, the SPL of the AoA=5° cases falls below the RAPL around 500 Hz. However, with these results, it is concluded that the acoustic advantage (silent flight) of the owl is reduced at AoA=10°, especially at 10 m/s freestream velocity. Furthermore, the maximum sound pressure values in all cases are seen at low frequencies. A possible explanation can be that the freestream velocity is not high enough to form high-frequency vortices or the AoA is too small to shed vortices in higher frequencies. Another notable point is seen in Figure 6b and Figure 6c cases, where the sound pressure levels are almost at the same level after 3000 Hz. This can be an outcome of the crosswise increase in the freestream velocity and the AoA (respectively for Figure 6b and 6c), which can affect the flow in the same way.

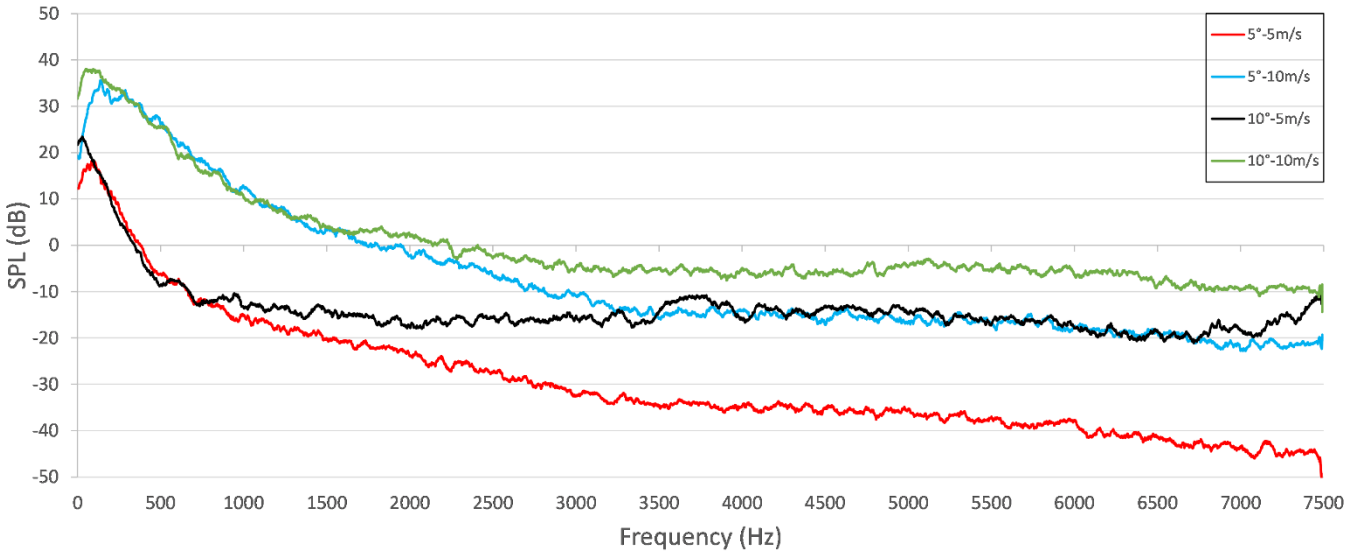

Figure 6 Sound pressure level between 0-7500 Hz for 5° and 10° AoA. Receiver is located at the trailing edge (0°). AoA=5° V=5 m/s (a) (red), AoA=5° V=10 m/s (b) (blue), AoA=10° V=5 m/s (c) (black), AoA=10° V=10 m/s (d) (green)

Liu et al. [23] found the maximum SPL (25-30 dB) at around 192 Hz for the similar owl airfoil in a numerical analysis (AoA=0°-9° and V= 7.5 m/s as boundary conditions), which verifies the results in this study. Also, the SPL distribution at 10 m/s freestream velocity for an owl airfoil obtained numerically by Li et al. [35] (23-40 dB) is similar to our results at the same velocity (i.e. 30-45 dB). The slight differences can be related to chord length, as Li et al. used 100 mm, whereas the chord length in our case is 150 mm. The experimental results in the study of Sarradj et al. [31] show that the maximum SPL for the owl and hawk is around 20 dB at regular flight speeds, which is comparable to our findings of 15-30 dB at 5 m/s. This can be compared with the 5 m/s data of this study because the flight speed range for the owl is around 2.5-10 m/s [9, 13].

In Figure 7 , the SPL distribution around the airfoil s are presented. The results are plotted for average SPL values at the receiver locations for the maximum frequency interval of the owl wing profile. These values are calculated to smooth out the fluctuating data at the maximum frequency interval and are referred to as overall sound pressure levels (OSPL) in this study. The maximum frequency intervals were mentioned in the previous section, where the range for Figure 7a is 20 – 120 Hz, for Figure 7b is 90 – 290 Hz, for Figure 7c is 15 – 70 Hz and for Figure 7d is 40 – 170 Hz.

For Figure 7a and Figure 7c cases, it can be said that the OSPL's lie between 26-28dB. With the increase of the velocity to 10 m/s, the OSPL increases to 45dB on average, which corresponds to an increase of approximately 15dB compared to the 5 m/s case. As an overview, between the receivers at 0°-340° (at trailing-edge pressure side region) and 140°-160° (at leading-edge suction side region), a same pattern of OSPL is noticed. A possible explanation can be that the vorticity characteristics at the leading and trailing edge have a similar effect on the sound pressure level. It is known that the flight speed range of the owl is around 2.5-10 m/s, which was also mentioned before in this study. Consequently, the OSPL behavior in 5 m/s freestream velocity conditions shows that the owl wing profile generates less noise compared to the 10 m/s conditions, regardless of the AoA.

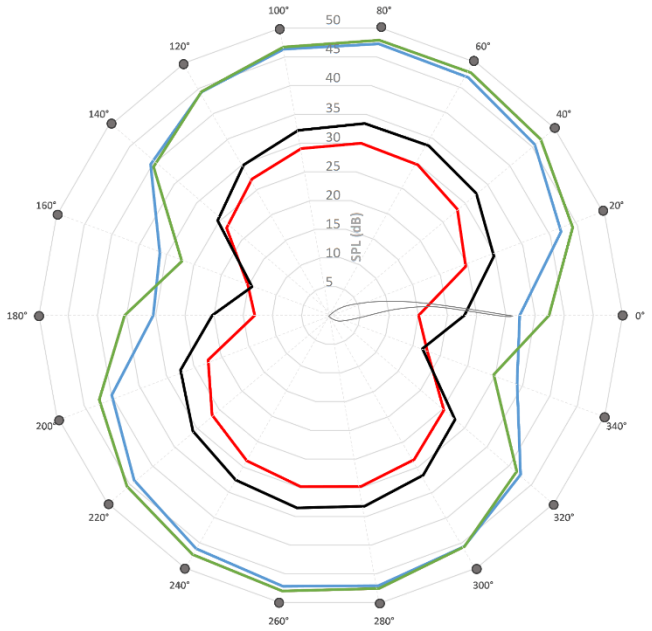

Figure 7 OSPL distribution around the owl airfoil. 5°AoA - 5 m/s (a)(red), 5°AOA - 10 m/s (b)(blue), 10°AOA - 5 m/s (c)(black), 10°AOA - 10 m/s (d)(green). Black dots represent the locations of the receivers. The frequency interval in the radar charts corresponds to the maximum SPL range. Airfoil is drawn to indicate the relative AoA with respect to the receivers. Therefore the chord length, and the distance between the leading edge of the airfoil and the receivers are not to scale

4. CONCLUSION

The objective of this study is to investigate the flow characteristics of the owl's wing profile, and its effect on the silent flight of the owls. For this purpose, typical values that describe the properties of the owl are chosen and analyzed with 2D computational fluid dynamics tools. In order to represent the gliding flight, freestream velocities are chosen as 2.5 m/s, 5 m/s, and 10 m/s, whereas the angle of attacks are taken as 0°, 5°, and 10°.

As a brief summary of both vorticity and acoustic results, it is seen that each investigated characteristic of the vortices have an impact on the SPL. The effect of the formation position of the vortices on the noise distribution can be seen in Figure 7. On the other hand, the vortex intensity and dimension have an influence on the SPL, whereas the vortex shedding (or occurrence frequency) is related to the frequency-dependent SPL (Figure 6). To understand the acoustic behavior of the owl wing profile, transient analyses are carried out over time. In general, the results show that all the cases with 2.5 m/s freestream velocity and 0° AoA have small vortices in the field, and almost no vortex interactions are observed. Since the vortices for 5 m/s and 10 m/s are larger and have more interaction between eachother, it is expected that the noise generation would be greater compared to 2.5 m/s. This can be seen in the vortex diameters, where it doubled from 2.5 m/s to 5 m/s, and almost tripled from 2.5 m/s to 10 m/s.

The results of the acoustic charachteristics of the owl airfoil show that in a frequency range between 0 – 2250 Hz, it generates the least noise at 5 m/s freestream velocity regardless of the AoA. The max SPL increases almost 80% from 5 m/s to 10 m/s, where the values share similarities with the literature. Investigations of the SPL distribution around the airfoil show that the owl has a similar sound distribution at the trailing-edge (at 0° and 340° receivers) and leading-edge (at 140° and 160° receivers). Thus, the flow behaviour at the leading and trailing edge are alike and affects the SPL in the same way. It is known that it has a flight speed range of 2.5-10 m/s ,

which explains why it generated more noise at 10 m/s freestream velocity conditions. Furthermore, the max SPL of the owl airfoil is located directly above and underneath the profile, whereas the min SPL is around the leading- and trailing-edge zone. In general, investigated flow characteristics around the owl wing profile are in agreement with the "nearly silent flight" observations of the owl.

Funding

The authors have no received any financial support for the research, authorship or publication of this study.

The Declaration of Conflict of Interest/ Common Interest

No conflict of interest or common interest has been declared by the authors.

Authors' Contribution

The first author contributed 60%, the second author 40%.

The Declaration of Ethics Committee Approval

This study does not require ethics committee permission or any special permission.

The Declaration of Research and Publication Ethics

The authors of the paper declare that they comply with the scientific, ethical and quotation rules of SAUJS in all processes of the paper and that they do not make any falsification on the data collected. In addition, they declare that Sakarya University Journal of Science and its editorial board have no responsibility for any ethical violations that may be encountered, and that this study has not been evaluated in any academic publication environment other than Sakarya University Journal of Science.

REFERENCES

[1] United States Civil Aeronautics Administration, "A Selected and Annotated Bibliography of Recent Air Age Education Textbooks," 1947.

[2] J. P. Fielding, Introduction to Aircraft Design. Cambridge University Press, 1999.

[3] K. P. Valavanis and G. J. Vachtsevanos, Handbook of unmanned aerial vehicles. Springer Netherlands, 2015.

[4] J. M. Forshaw, Encyclopaedia of Animals: Birds. Murdoch Books UK, 1991.

[5] H. Hertel, Struktur, Form, Bewegung. Mainz: Krauskopf-Verlag, 1963.

[6] T. Bachmann, G. Mühlenbruch, and H. Wagner, "The barn owl wing: an inspiration for silent flight in the aviation industry?," in Bioinspiration, Biomimetics, and Bioreplication, 2011, p. 79750N.

[7] J. del Hoyo, A. Elliott, and J. Sargatal, "Handbook of the Birds of the World. Ostrich to Ducks," Ostrich to Ducks. 1992.

[8] R. Sale, Falcons. Harper Collins UK, 2016.

[9] W. Scherzinger and T. Mebs, Die Eulen Europas. Franckh-Kosmos Verlag, 2000.

[10] H. N. Southern and H. Mikkola, "Owls of Europe," J. Anim. Ecol., 1984.

[11] C.-T. Edward L. and J. Roskam, Airplane Aerodynamics and Performance, 5th ed. DARcorporation, 1997.

[12] T. Liu, K. Kuykendoll, R. Rhew, and S. Jones, "Avian wing geometry and kinematics," AIAA J., 2006.

[13] W. Neuhaus, H. Bretting, and B. Schweizer, "Morphologische und Funktionelle Untersuchungen Über den Lautlosen Flug Der Eulen (Strix Aluco) im Vergleich zum Flug Der Enten (Anas Platyrhynchos)," Biol. Zent. Bl., 1973.

[14] S. Ito, "Aerodynamic influence of leading-edge serrations on an airfoil in a low Reynolds number: A study of an owl wing with leading edge serrations," J. Biomech. Sci. Eng., 2009.

[15] E. Mascha, "Über die Schwungfedern," Zeitschrift für wissenschaftliche Zool., no. 77, pp. 606–651, 1904.

[16] T. Geyer, E. Sarradj, and C. Fritzsche, "Measuring owl flight noise," in INTERNOISE 2014 - 43rd International Congress on Noise Control Engineering: Improving the World Through Noise Control, 2014.

[17] K. Kondo et al., "Analysis of Owl-like Airfoil Aerodynamics at Low Reynolds Number Flow," Trans. JAPAN Soc. Aeronaut. Sp. Sci. Aerosp. Technol. JAPAN, 2014.

[18] K. Kondo, H. Aono, T. Nonomura, A. Oyama, K. Fujii, and M. Yamamoto, "Large-eddy simulations of owl-like wing under low reynolds number conditions," in American Society of Mechanical Engineers, Fluids Engineering Division (Publication) FEDSM, 2013.

[19] M. Anyoji, S. Wakui, D. Hamada, and H. Aono, "Experimental Study of Owl-Like Airfoil Aerodynamics at Low Reynolds Numbers," J. Flow Control. Meas. & Vis., 2018.

[20] S. B. Pope, Turbulent Flows. Cambridge University Press, 2000.

[21] T. Bensow, R. E., Fureby, C., Liefvendahl, C. & Persson, "A Comparative Study of RANS, DES and LES," 26th ONR Symp. Nav. Hydrodyn., 2006.

[22] A. Fluent, "Ansys Fluent Theory Guide," ANSYS Inc., USA, 2013.

[23] X. Liu and X. Liu, "A Numerical Study of Aerodynamic Performance and Noise of a Bionic Airfoil Based on Owl Wing," Adv. Mech. Eng., 2014.

[24] P. R. Spalart and S. R. Allmaras, "One-equation turbulence model for aerodynamic flows," Rech. Aerosp., no. 1, pp. 5-21, 1994.

[25] M. J. Lighthill, "On sound generated aerodynamically I. General theory," Proc. R. Soc. London. Ser. A. Math. Phys. Sci., 1952.

[26] WILLIAMS JEF and HAWKINGS DL, "Sound Generation by Turbulence and Surfaces in Arbitrary Motion," Roy Soc London-Philosophical Trans Ser A, 1969.

[27] M. P. Norton and D. G. Karczub, Fundamentals of Noise and Vibration Analysis for Engineers. 2003.

[28] G. Tucker, V.; Parrot, "Aerodynamics of Gliding Flight in a Falcon and Other Birds," J. Exp. Biol., 1970.

[29] T. Wolf and R. Konrath, "Avian wing geometry and kinematics of a free-flying barn owl in flapping flight," Exp. Fluids, 2015.

[30] T. Geyer, E. Sarradj, and C. Fritzsche, "Silent owl flight: Comparative acoustic wind tunnel measurements on prepared wings," Acta Acust. united with Acust., 2013.

[31] E. Sarradj, C. Fritzsche, T. Geyer, and E. Gutmark, "Silent OWL flight: Bird flyover noise measurements," AIAA J., 2011.

[32] J. Kopania, "Acoustics Parameters the Wings of Various Species of Owls," Inter-Noise Noise-Con Congr. Conf. Proc., pp. 6841–7829, 2016.

[33] T. Geyer, E. Sarradj, and C. Fritzsche, "Measurement of the noise generation at the trailing edge of porous airfoils," Exp. Fluids, 2010.

[34] J. Vad, G. Koscsó, M. Gutermuth, Z. Kasza, T. Tábi, and T. Csörgo, “Study of the aero-acoustic and aerodynamic effects of soft coating upon airfoil,” JSME Int. Journal, Ser. C Mech. Syst. Mach. Elem. Manuf., 2007.

[35] D. Li and X. Liu, “Aerodynamic performance and acoustic characteristics of bionic airfoil inspired by three-dimensional long-eared owl wing under low reynolds number,” in Proceedings of the ASME Turbo Expo, 2016.

[36] H. Roeser, R. J.; Valente, Michael ; Hosford-Dunn, Audiology Diagnosis, 2nd ed. Thieme, 2007.